DEUTSCHES ELEKTRONEN – SYNCHROTRON

DESY 92-013
January 1992

Search for Neutrinoless τ Decays

The ARGUS Collaboration

ISSN 0418-9833

NOTKESTRASSE 85 · D - 2000 HAMBURG 52

To be sure that your preprints are promptly included in the HIGH ENERGY PHYSICS INDEX, send them to the following (if possible by air mail):

DESY Bibliothek Notkestraße 85 W-2000 Hamburg 52 Germany	DESY-IfH Bibliothek Platanenallee 6 O-1615 Zeuthen Germany

DESY 92-013
January 1992

ISSN 0418-9833

Search for Neutrinoless τ Decays

The ARGUS Collaboration

H. Albrecht, H. Ehrlichmann, T. Hamacher, A. Krüger, A. Nau, A. Nippe, S. Nowak[1], M. Reidenbach, M. Schäfer, H. Schröder, H. D. Schulz, M. Walter[1], R. Wurth
DESY, Hamburg, Germany

R. D. Appuhn, C. Hast, G. Herrera, H. Kolanoski, A. Lange, A. Lindner, R. Mankel, M. Schieber, T. Siegmund, B. Spaan, H. Thurn, D. Töpfer, A. Walther, D. Wegener
Institut für Physik[2], Universität Dortmund, Germany

M. Paulini, K. Reim, H. Wegener
Physikalisches Institut[3], Universität Erlangen-Nürnberg, Germany

R. Mundt, T. Oest, W. Schmidt-Parzefall
II. Institut für Experimentalphysik, Universität Hamburg, Germany

W. Funk, J. Stiewe, S. Werner
Institut für Hochenergiephysik[4], Universität Heidelberg, Germany

K. Ehret, A. Hölscher, W. Hofmann, A. Hüpper, S. Khan, K. T. Knöpfle, J. Spengler
Max-Planck-Institut für Kernphysik, Heidelberg, Germany

D. I. Britton[5], C. E. K. Charlesworth[6], K. W. Edwards[7], E. R. F. Hyatt[5], H. Kapitza[7], P. Krieger[8,6], D. B. MacFarlane[5], P. M. Patel[5], J. D. Prentice[6], P. R. B. Saull[5], S. C. Seidel[6], K. Tzamariudaki[5], R. G. Van de Water[6], T.-S. Yoon[6]
Institute of Particle Physics[9], Canada

D. Reßing, M. Schmidtler, M. Schneider, K. R. Schubert, K. Strahl, R. Waldi, S. Weseler
Institut für Experimentelle Kernphysik[10], Universität Karlsruhe, Germany

G. Kernel, P. Križan, E. Križnič, T. Podobnik, T. Živko
Institut J. Stefan and Oddelek za fiziko[11], Univerza v Ljubljani, Ljubljana, Slovenia

H. I. Cronström, L. Jönsson
Institute of Physics[12], University of Lund, Sweden

V. Balagura, I. Belyaev, M. Danilov, A. Droutskoy, A. Golutvin, I. Gorelov, G. Kostina, V. Lubimov, P. Murat, P. Pakhlov, F. Ratnikov, S. Semenov, V. Shibaev, V. Soloshenko, I. Tichomirov, Yu. Zaitsev
Institute of Theoretical and Experimental Physics, Moscow, Russia

[1] DESY, IfH Zeuthen

[2] Supported by the German Bundesministerium für Forschung und Technologie, under contract number 054DO51P.

[3] Supported by the German Bundesministerium für Forschung und Technologie, under contract number 054ER12P.

[4] Supported by the German Bundesministerium für Forschung und Technologie, under contract number 055HD21P.

[5] McGill University, Montreal, Quebec, Canada.

[6] University of Toronto, Toronto, Ontario, Canada.

[7] Carleton University, Ottawa, Ontario, Canada.

[8] Supported in part by the Walter C. Sumner Foundation.

[9] Supported by the Natural Sciences and Engineering Research Council, Canada.

[10] Supported by the German Bundesministerium für Forschung und Technologie, under contract number 054KA17P.

[11] Supported by the Department of Science and Technology of the Republic of Slovenia and the Internationales Büro KfA, Jülich.

[12] Supported by the Swedish Research Council.

Abstract

Upper limits on branching ratios for six neutrinoless leptonic, 16 semileptonic, two radiative-leptonic, two radiative-hadronic and three purely hadronic τ decays have been determined. The results improve over previously published ones by about a factor of two. For the first time the lepton and baryon number violating decays $\tau^- \to \bar{p}\,\gamma$, $\tau^- \to \bar{p}\,\pi^0$ and $\tau^- \to \bar{p}\,\eta$ have been investigated. The 90% confidence level (CL) limits for the corresponding branching ratios amount to 2.9×10^{-4}, 6.6×10^{-4} and 1.3×10^{-3} respectively.

1 Introduction

The standard model of elementary particle physics assigns each lepton and quark a flavour quantum number. A particular lepton flavour is shared by the charged and neutral leptons of one family. In the quark sector, weak charged currents induce transitions within one, or between two different families, while for the lepton sector flavour changing currents have not been observed. The recent claim [1] of a weak coupling between the electron neutrino and a heavy neutrino with a mass of 17 keV has revived interest in lepton flavour-violating transitions.

τ lepton decays are an advantageous place for such searches. The large mass of the τ lepton allows access to many more final states than for other leptons. Moreover, for τ decays the final state can be purely hadronic (e.g. $\tau^- \to \bar{p}\,\pi^0$). Many extensions of the standard model exist which predict lepton flavour violation in different final states. Therefore, a study of τ decays allows a much broader confrontation of these predictions with experimental data.

In this paper we describe the results of an analysis based on nearly twice the data sample used for our previous publication [2]. Moreover, a large number of new channels have been added to the search, bringing the number investigated to a total of 29 different neutrinoless τ decays. A detailed description of the analysis is given in [3].

The data used in this analysis were collected with the ARGUS detector at the DORIS II electron-positron storage ring at DESY. The detector is described in detail in [4]. Luminosity was recorded at different center-of-mass energies corresponding to the $\Upsilon(1S)$, $\Upsilon(2S)$ and $\Upsilon(4S)$ resonances as well as to the nearby continuum. In this analysis, the data sample consists of 374 300 τ pairs, corresponding to an integrated luminosity of 387 pb^{-1}.

The basic search technique is to examine the invariant mass distribution of the final state for a given search channel in the region of the τ mass, after imposing kinematic cuts and particle identification requirements. Charged hadrons can be identified both by the measurement of the specific ionization (dE/dx) in the main drift chamber and by the measurement of the velocity in the time-of-flight (TOF) system. In order to identify electrons, the observed

energy deposition in the electromagnetic calorimeter, the number of shower counters assigned to the track and the lateral shape of the distribution are used in combination with dE/dx and TOF to calculate a combined likelihood [5]. Muons were likewise identified using all detector information, but are also required to have at least one assigned hit in the outer layers of the muon chambers.

2 Search for neutrinoless 3-prong decays of τ leptons

In this section results are presented for the following leptonic and semileptonic neutrinoless τ decays with three charged particles in the final state[1]:

1.	$\tau^- \to e^-e^+e^-$	7.	$\tau^- \to e^-\pi^+\pi^-$	13.	$\tau^- \to e^-\pi^+K^-$
2.	$\tau^- \to e^-\mu^+\mu^-$	8.	$\tau^- \to e^+\pi^-\pi^-$	14.	$\tau^- \to e^+\pi^-K^-$
3.	$\tau^- \to e^+\mu^-\mu^-$	9.	$\tau^- \to \mu^-\pi^+\pi^-$	15.	$\tau^- \to \mu^-\pi^+K^-$
4.	$\tau^- \to \mu^-e^+e^-$	10.	$\tau^- \to \mu^+\pi^-\pi^-$	16.	$\tau^- \to \mu^+\pi^-K^-$
5.	$\tau^- \to \mu^+e^-e^-$	11.	$\tau^- \to e^-\rho^0$	17.	$\tau^- \to e^-K^{*0}$
6.	$\tau^- \to \mu^-\mu^+\mu^-$	12.	$\tau^- \to \mu^-\rho^0$	18.	$\tau^- \to \mu^-K^{*0}$

The search demands a 1-versus-3 topology for the τ pair, where one τ decays into a single charged and one or more neutral particles according to the standard model (referred to here as the standard 1-prong decay), while lepton flavour violation was assumed on the 3-prong side:

$$e^+e^- \longrightarrow \tau^+\tau^- \begin{cases} \longrightarrow e^-e^+e^-,\ e^-\mu^+\mu^-,\ \ldots \\ \longrightarrow e^+\nu_e\overline{\nu}_\tau,\ \ \mu^+\nu_\mu\overline{\nu}_\tau,\ \pi^+\overline{\nu}_\tau,\ K^+\overline{\nu}_\tau,\ \rho^+\overline{\nu}_\tau,\ a_1^+\overline{\nu}_\tau,\ K^{*+}\overline{\nu}_\tau. \end{cases}$$

Events are required to have exactly four charged particles with zero total charge. No more than three photons with energy $E_\gamma > 0.08\ GeV$ are allowed. Each charged particle must point to the main vertex, is required to have a transverse momentum of $p_{trans} > 0.06\ GeV/c$ and a polar angle with respect to the beam direction in the range $|\cos\theta| < 0.92$. Since the τ pairs are produced back-to-back with momenta of $\approx 4.7\ GeV/c$, their decay products travel mainly in opposite directions. This characteristic 1-versus-3 topology of the four charged particles is selected by requiring that one charged track in an event lies in a hemisphere opposite to the other 3 charged tracks,

$$\cos(\vec{p}_1, \vec{p}_i) \ < \ 0 \qquad i = 2,3,4\,.$$

[1]References in this paper to a specific charged state also imply the charge conjugate state.

In addition, the opening angle between the momentum sum of the three charged particles with respect to the 1-prong candidate must be at least 120°,

$$\cos\left(\vec{p}_1, \sum_2^4 \vec{p}_i\right) \ < \ -0.5$$

where $\vec{p}_1$ denotes the 1-prong momentum and $\vec{p}_i$ the momenta of the particles on the 3-prong side.

These cuts reduce the number of 4-prong events to 119 321 with an efficiency of 35% for neutrinoless τ decays into three charged particles. In addition to the events of interest, background contributions from radiative QED, $q\overline{q}$ and $\gamma\gamma$ events, as well as ggg and τ decays, are present. Beam-gas and beam-wall background is negligible.

2.1 Background reduction

Further cuts are applied to the data in order to enhance the signal-to-background ratio as determined by Monte Carlo (MC) simulation ($q\overline{q}$, ggg events and standard τ decays) or special data samples, e.g. $\gamma\gamma$ events and radiative Bhabha events where the photon converts into an e^+e^- pair. The latter are obtained by independent selection criteria to the primary τ pair sample. The neutrinoless τ decays are simulated assuming a phase-space distribution. The particular combination of cuts used varies from channel to channel, reflecting the different levels of predicted background and effectiveness of particle identification in each case.

- **Cut No. 1**: Contributions from converted photons due to radiative QED events are reduced by rejecting events where the invariant mass of oppositely charged particles (compatible with the electron hypothesis) on the 3-prong side is smaller than 100 MeV/c^2:

$$m_{e^+e^-} > 100\ MeV/c^2\,.$$

- **Cut No. 2**: The normalized sum of electromagnetic shower energy and momentum for the 1-prong is correlated for Bhabha events with the opening angle between the observed total momentum of the event and the beam direction $\vec{e}_b$. Figure 1 shows r_1 versus $\cos\theta_{ptot}$, where

$$r_1 \ = \ \frac{\left(E^{shower}_{1-prong} + |\,\vec{p}_{1-prong}\,|\right)}{E_{cm}}\,,$$

$$\cos\theta_{ptot} = \vec{e}_b \cdot \frac{\vec{p}_{tot}}{|\,\vec{p}_{tot}\,|}\,,$$

for the data (fig. 1a) and for simulated neutrinoless τ decays (fig. 1b). Only a weak correlation is observed for the latter. Hence the requirement

$$r_1 < 1 - \cos^2\theta_{ptot}$$

reduces the Bhabha background considerably, while only marginal losses are expected for the search channels.

- **Cut No. 3**: For a neutrinoless τ decay into three charged particles the 3-prong momentum should equal the τ momentum. In a plot of the scaled 3-prong momentum

$$r_2 = \frac{|\vec{p}_{3prong}|}{E_{cm}}$$

versus r_1, as shown in fig. 2a and 2b, neutrinoless τ decays are well separated from $\gamma\gamma$ events at the bottom left and Bhabha events at the top right. Standard τ decays, $q\bar{q}$ and ggg events populate the intermediate region. The requirement

$$r_2 > 0.273 \cdot r_1 + 0.3$$

completely removes the $\gamma\gamma$ events and further reduces Bhabha background.

These cuts eliminate the background which might simulate the leptonic neutrinoless τ decays 1 – 6. In the case of the semileptonic search channels 7 – 18, the background from standard semileptonic τ decays and $q\bar{q}$ events must be further suppressed. Also, Bhabha events remain a significant contribution due to misidentification of electrons as final state hadrons.

- **Cut No. 4**: The copious production of radiative Bhabha events, which normally have a low 3-prong mass, becomes a significant background when the use of an hadronic mass through misidentification raises the apparent 3-prong mass into the region around the τ mass. Therefore, for channels 7 - 18, events with an electron on the 1-prong side are rejected.

- **Cut No. 5**: Further discrimination against standard τ and $q\bar{q}$ events can be obtained by utilizing the near hermeticity of the ARGUS detector.

  The missing momentum, defined to be equal to minus the total momentum of all measured particles, for the events of interest is dominated by the neutrinos accompanying the standard 1-prong τ decay. The energy of the neutrinos can be determined by subtracting the energy of all measured particles on the 1-prong side from the beam energy, since this is the known energy of the τ lepton. Hence, the missing four-momentum, assumed to originate from the neutrinos in the 1-prong decay, is

$$p^{\mu}_{miss} = \begin{pmatrix} E_{beam} - E_{single} \\ -\vec{p}_{tot} \end{pmatrix}.$$

Using this technique, and including all photons within a cone of 70° with respect to the 1-prong direction, one can determine the invariant mass of the 1-prong side. This mass

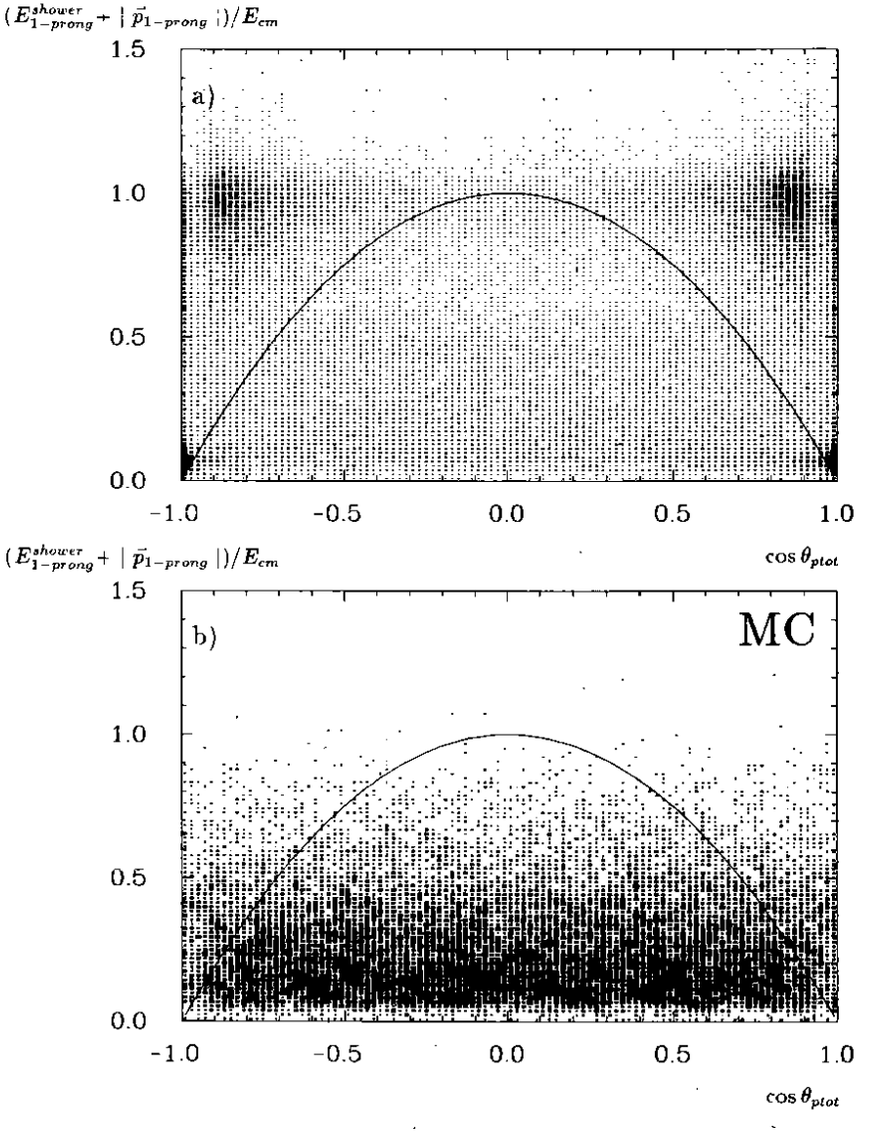

Figure 1: $(E^{shower}_{1-prong} + |\vec{p}_{1-prong}|)/E_{cm}$ versus $\cos\theta_{ptot}$ after preselection for a) data and b) neutrinoless τ decays. Events above the parabola are discarded.

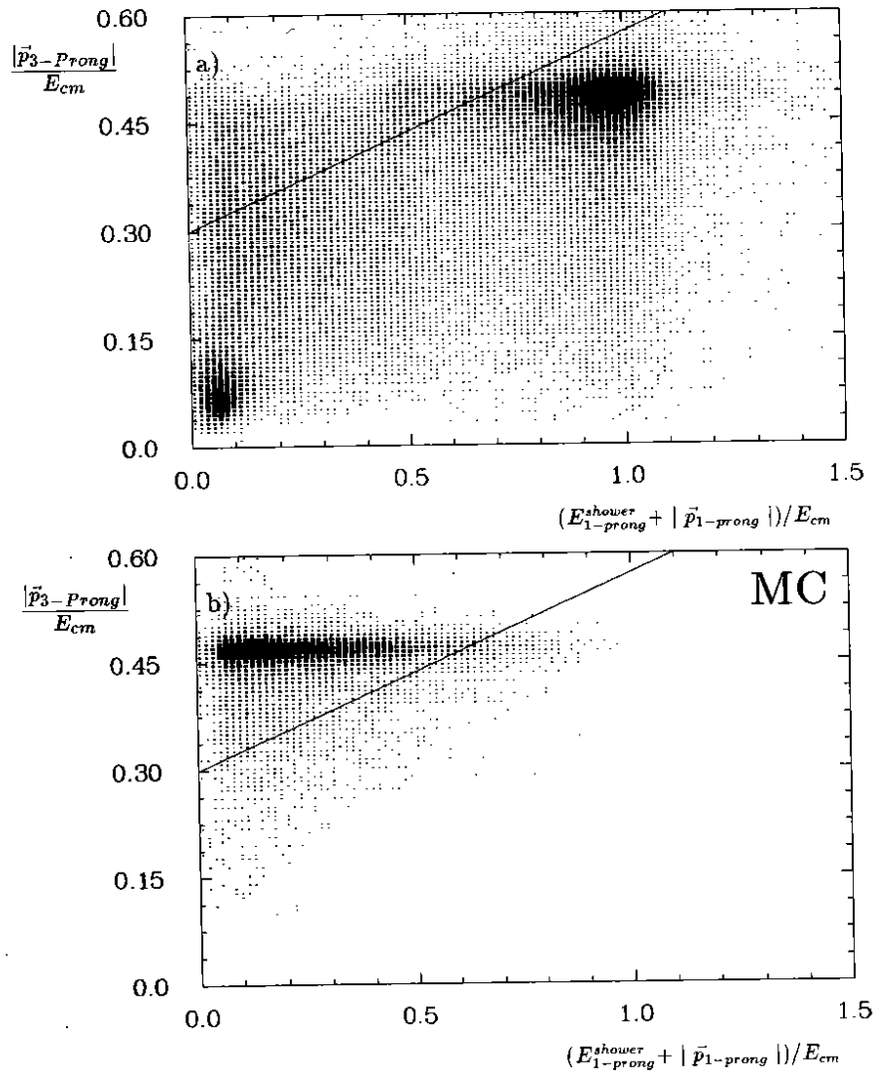

Figure 2: $|\vec{p}_{3-Prong}|$ versus $(E^{shower}_{1-prong} + |\vec{p}_{1-prong}|)/E_{cm}$ for a) data and b) neutrinoless τ decays after preselection. Events below the solid line are discarded.

should equal the τ mass, given our assumptions. With the subscript *single* denoting quantities for all measured particles on the 1-prong side:

$$m^2_{\tau-1-Prong} = p^{\mu 2}_{\tau\ 1-Prong} = (p^{\mu}_{single} + p^{\mu}_{miss})^2$$

For simulated neutrinoless events the distribution in fig. 3 peaks at the square of the τ mass, or 3.18 GeV^2/c^4, whereas the background is much broader. The requirement

$$2\ \frac{GeV^2}{c^4} < m^2_{\tau-1-prong} < 7\ \frac{GeV^2}{c^4}$$

removes those events with large m^2 values, which are more likely to be standard τ pair or $q\bar{q}$ events since their missing momenta are not correlated with the 1-prong side. In addition, Bhabha events with small m^2 values are suppressed.

For channels which still have some background at this point, the sensitivity can be improved by exploiting the fact that the energy of the neutrinoless 3-prong side should be equal to the beam energy. We require this to be the case within 3 standard deviations:

$$|\ E_{3-prong} - E_{beam}\ | < 3\sigma_E\ .$$

Events fulfilling this condition are subjected to a 1-constraint fit, where the invariant mass and the momentum of the 3-prong side are adjusted to satisfy:

$$E_{beam} = \sqrt{m^2_{3-prong} + |\ \vec{p}_{3-prong}\ |^2}\ .$$

2.2 Results

The final cuts applied in each decay channel are collected in table 1. For most of the search modes no events consistent with neutrinoless τ decays survive in the signal region, defined to be $\pm$ 2 standard deviations around the nominal τ mass. The expected width is derived by a Monte Carlo calculation. If one takes into account the selection efficiency[2] ϵ_{sel} derived by applying the cuts to simulated events, the trigger efficiency ($\sim$ 90%) and the losses due to faked photons (1%) [6], one arrives at the 90% CL limits given in table 1. Note that the total efficiencies ϵ_{tot} include the applied particle identification requirements, which, in conjunction with the described kinematic cuts, are required to achieve good sensitivity for neutrinoless τ decays [3]. In some cases the particle identification has a much lower efficiency than any one

[2]The relative errors of all efficiencies listed in this paper are less than 10%

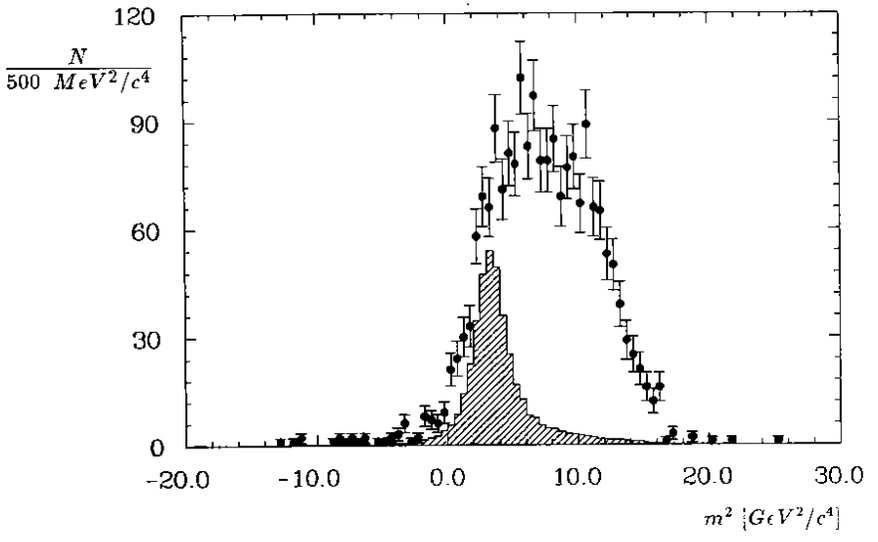

Figure 3: $m^2_{\tau-1-prong}$ for data after application of cuts 1 – 4 (with error bars) and for neutrinoless Monte Carlo τ decays (hatched histogram)

of the kinematic cuts. A rough estimate of the identification efficiencies can be obtained by comparing the selection efficiency ϵ_{sel}, also given in the table, to the total efficiency ϵ_{tot}.

The mass spectra on the 3-prong side for all channels are given in fig. 4 – 6. The distributions are found to correspond to expectations for typical background sources, i.e. they are evenly populated due to $q\bar{q}$ or Bhabha background, while standard τ decays contribute with a broad signal below the τ mass. Note that the τ contribution should die out at 1.8 GeV, but can be shifted higher or lower in mass due to incorrect particle identification. Since there is no enhancement close to the mass of the τ lepton, we conclude that there is no evidence for neutrinoless τ decays into three charged particles.

No.	Decay channel	Cuts	ϵ_{sel}[%]	ϵ_{tot}[%]	N_{seen}	Upper limit [10^{-5}]
1.	$\tau^- \to e^- e^- e^-$	1 2 3	27.9	23.1	0	1.3
2.	$\tau^- \to e^- \mu^+ \mu^-$	1 2 3	27.9	16.4	0	1.9
3.	$\tau^- \to e^- \mu^- \mu^-$	1	34.6	16.9	0	1.8
4.	$\tau^- \to \mu^- e^+ e^-$	1 2 3	27.9	22.5	0	1.4
5.	$\tau^- \to \mu^+ e^- e^-$	1 2 3	27.9	21.8	0	1.4
6.	$\tau^- \to \mu^- \mu^- \mu^-$	1	34.6	16.1	0	1.9
7.	$\tau^- \to e^- \pi^+ \pi^-$	1 2 3 4 5	16.5	11.4	0	2.7
8.	$\tau^- \to e^+ \pi^- \pi^-$	1 2	31.6	17.5	0	1.8
9.	$\tau^- \to \mu^- \pi^+ \pi^-$	1 2 3 5	20.5	8.6	0	3.6
10.	$\tau^- \to \mu^+ \pi^- \pi^-$	1 2 3 5	20.5	8.2	1	6.3
11.	$\tau^- \to e^- \rho^0$	1 2 3	27.9	16.6	0	1.9
12.	$\tau^- \to \mu^- \rho^0$	1 2 3 5	20.5	10.7	0	2.9
13.	$\tau^- \to e^- \pi^+ K^-$	1 2 3 4 5	16.5	10.4	0	2.9
14.	$\tau^- \to e^+ \pi^- K^-$	1 2	31.6	15.2	0	2.0
15.	$\tau^- \to \mu^- \pi^- K^-$	1 2 3 4 5	16.5	5.3	2	11
16.	$\tau^- \to \mu^+ \pi^- K^-$	1 2 3 4 5	16.5	5.3	0	5.8
17.	$\tau^- \to e^- K^{*0}$	1 2 3 4 5	16.5	8.1	0	3.8
18.	$\tau^- \to \mu^- K^{*0}$	1 2 3 5	20.5	6.9	0	4.5

Table 1: Results of searches for leptonic and semileptonic neutrinoless τ decays into three charged particles

3 Search for neutrinoless τ decays into one charged and one neutral particle

We have searched for neutrinoless 1-prong τ decays in events of the following type:

$$e^+e^- \to \tau^+\tau^-$$
$$\longrightarrow e^-\gamma,\ e^-\pi^0,\ e^-\eta,\ \mu^-\gamma,\ \mu^-\pi^0,\ \mu^-\eta,\ \pi^-\gamma,\ \pi^-\pi^0,\ \bar{p}\gamma,\ \bar{p}\pi^0,\ \bar{p}\eta$$
$$\longrightarrow e^-\nu_e\nu_\tau,\ \mu^-\nu_\mu\bar{\nu}_\tau,\ \pi^-\nu_\tau,\ K^-\bar{\nu}_\tau,\ \rho^-\bar{\nu}_\tau,\ a_1^-\bar{\nu}_\tau$$
$$\longrightarrow \pi^-\pi^0 \longrightarrow \pi^-\pi^0\pi^0.$$

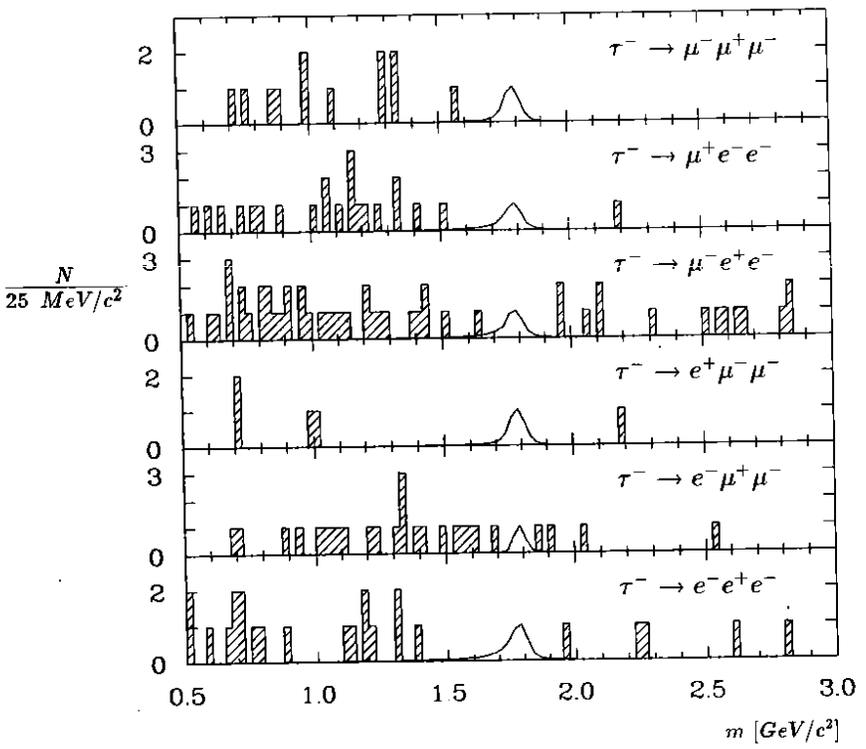

Figure 4: Invariant 3-prong masses for the decay channels 1 – 6, with corresponding resolution function (solid line)

The main background for these decays comes from radiative Bhabha and μ-pair production, where one of the final state leptons radiates a photon:

$$e^+e^- \to e^+e^-\gamma,\ \mu^+\mu^-\gamma.$$

After the reduction of radiative QED events, standard τ events remain as a background source, particularly for hadronic neutrinoless τ decays. Contributions from $q\bar{q}$ and $\gamma\gamma$ events are negligible, since 2-prong events are rare in $q\bar{q}$ fragmentation, and $\gamma\gamma$ events are suppressed by constraining the neutrinoless 1-prong side to the beam energy, as in the previous 3-prong analysis.

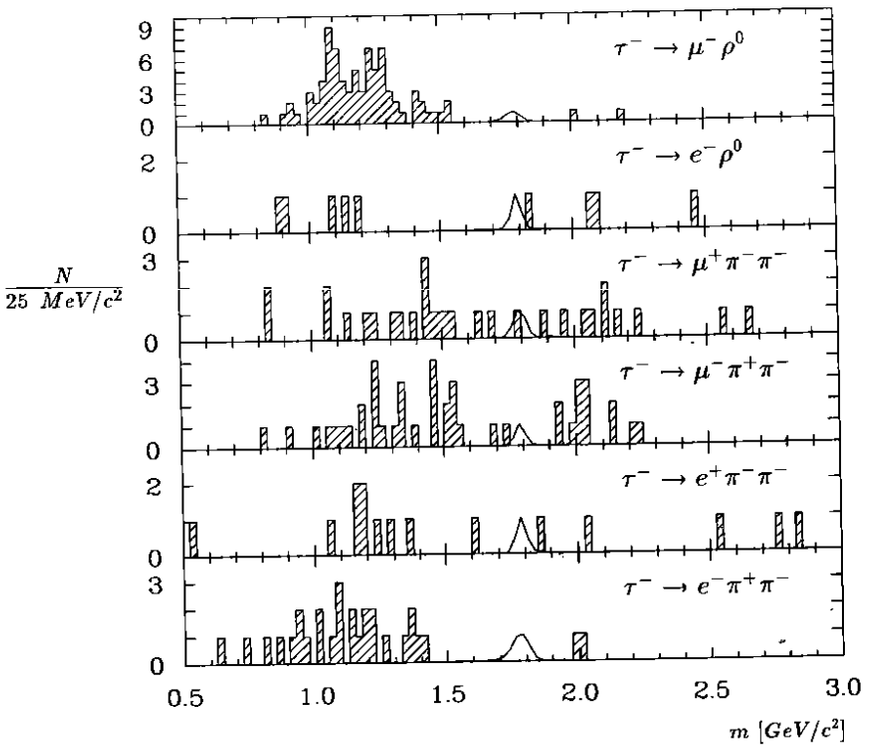

Figure 5: Invariant 3-prong masses for the decay channels 7 – 12, with corresponding resolution function (solid line)

3.1 Data selection

The analysis starts from a data set of 5.37×10^6 2-prong events which are selected by applying an initial set of cuts to reduce the Bhabha background:

- At least one of the charged tracks must lie outside of 30° from the beam axis.

In addition, one or more of the following conditions must be satisfied:

- At least one charged track with an electromagnetic shower energy

$$E^{shower} < 1.5\ GeV$$

or a momentum and a shower energy of

$$p > 3\ GeV/c \ \ and \ \ E^{shower} < 4\ GeV\,.$$

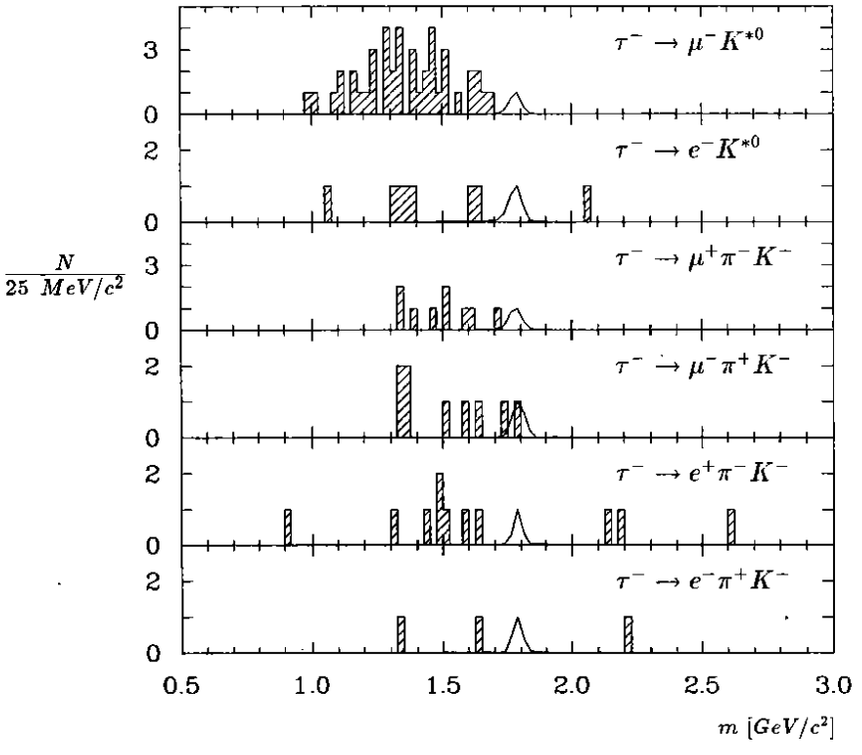

Figure 6: Invariant 3-prong masses for the decay channels 13 – 18, with corresponding resolution function (solid line)

- The two tracks are non-collinear by more than 15°
- The dE/dx value of one track is incompatible with that expected for an electron.

The preselection is completed by requiring events to have exactly two charged tracks with total charge zero, and at least one photon with $E_\gamma > 0.08\ GeV$. Again, as in section 2, each track is required to point to the main vertex and to have a transverse momentum of $p_{trans} > 0.06\ GeV/c$. Only charged particles with a polar angle with respect to the beam direction of $|\cos\theta| < 0.92$ are considered.

The major problem in the search for events with a neutrinoless τ decay into one charged and one neutral particle recoiling against a standard 1-prong τ decay accompanied by neutrinos, is to identify which of the two hemispheres is the potential candidate for a neutrinoless

τ decay. In this analysis, the missing momentum, i.e. minus the total momentum of all measured particles, is used to discriminate. For the events of interest, the missing momentum should fall into the hemisphere of the standard τ decay, while the recoil charged track, which is required to lie within 90° of the total momentum direction, is assumed to be due to a neutrinoless decay. These cuts retain 1.01×10^6 events, with an efficiency of 49% for neutrinoless τ decays into one charged and one neutral particle, averaged over the search set. For further analysis the study is broken into three classes as follows:

19. $\tau^- \to \mu^- \gamma$	25. $\tau^- \to e^- \eta$	27. $\tau^- \to \bar{p}\ \gamma$
20. $\tau^- \to \mu^- \pi^0$	26. $\tau^- \to \mu^- \eta$	28. $\tau^- \to \bar{p}\ \pi^0$
21. $\tau^- \to e^- \gamma$		29. $\tau^- \to \bar{p}\ \eta$
22. $\tau^- \to e^- \pi^0$		
23. $\tau^- \to \pi^- \gamma$		
24. $\tau^- \to \pi^- \pi^0$		

3.2 Search for the channels $\tau^- \to e^- \gamma,\ \mu^- \gamma,\ e^- \pi^o,\ \mu^- \pi^0,\ \pi^- \gamma,\ \pi^- \pi^0$

For these channels, since no restriction on the number of photons is possible, the main difficulty is distinguishing photons which satisfy conditions imposed by the kinematics of a neutrinoless decay, from those due to bremsstrahlung or the standard 1-prong τ decay. In order to reduce the contamination from bremsstrahlung, the photon energy is required to be

$$E_\gamma > 0.1 \cdot E_{cm}$$

which is still reasonably efficient for the search channels. This cut suppresses the main background sources for channels 19 – 24, namely radiative Bhabha events and μ-pairs, by a few orders of magnitude, while also reducing multiple counting. Energy clusters with more than 1 GeV are treated as π^0 mesons, since the granularity of the ARGUS electromagnetic calorimeter does not allow efficient separation of the decay photons above this energy.

A second condition exploits the observation that decay photons (π^0 mesons) from neutrinoless τ decays in channels 19 – 24 peak in the angular range

$$0.5 < \cos(\gamma, charged\ track) < 0.8\,,$$

with respect to the charged particle of the neutrinoless decay, while bremsstrahlung photons appear at small angles as shown in fig. 7. Finally, the energy of the charged track and the neutral particle is required to be consistent with the beam energy within 3 standard deviations. This requirement is used for all remaining 1-prong channels:

$$|\ E_{\gamma,charged} - E_{beam}\ | < 3\sigma_E\,.$$

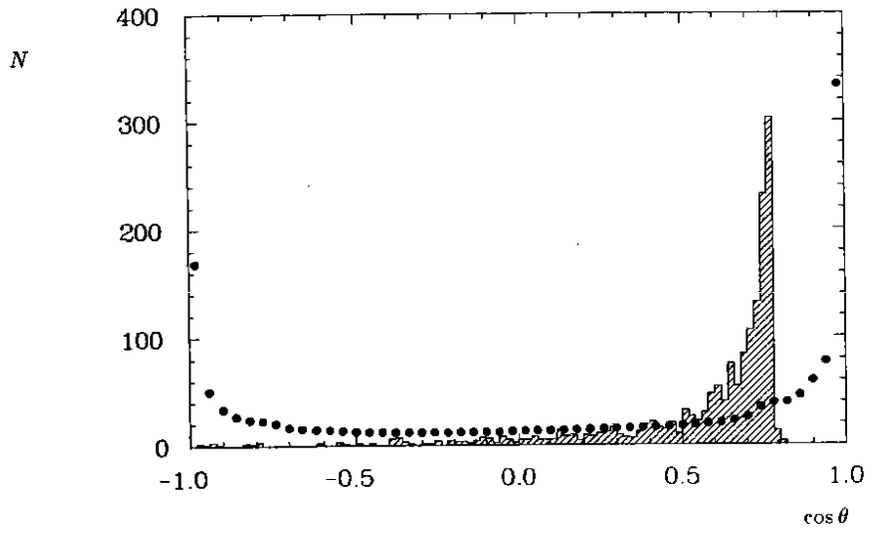

Figure 7: Distribution of the opening angle between the photon and lepton from neutrinoless τ decay channels 19 – 24 (hatched histogram) and data (dotted line) after preselection

The beam-energy constraint fit is applied to the neutrinoless side of the event, as described in section 2.2. A total of 21 074 events pass these requirements.

Further specific cuts are then introduced to suppress the remaining background.

- **Cut No. 1**: All decay products of radiative events are generally visible in the detector, while a standard 1-prong τ decay leads to a missing transverse momentum. The condition

$$\frac{|\vec{p}_{trans}|}{E_{cm}} > 0.03$$

reduces this background appreciably.

- **Cut No. 2**: A requirement similar to cut no. 2 of section 2.1 is made. In order to be efficient for both radiative Bhabha and μ-pair events, which have small shower counter deposition, the actual variables used are slightly modified. Thus, instead of $(E^{shower}_{1-prong} + |\vec{p}_{1-prong}|)$, only the 1-prong momentum, which is also large for μ-pair events, is used:

$$\frac{|\vec{p}_{1-pr}|}{E_{beam}} < 0.8 - \cos^2\theta_{ptot}\,.$$

This cut effectively suppresses radiative μ-pair and Bhabha events which peak at $|\vec{p}_{1-prong}|/E_{beam} \approx 1$ and $|cos\ \theta_{ptot}| \approx 0.9$.

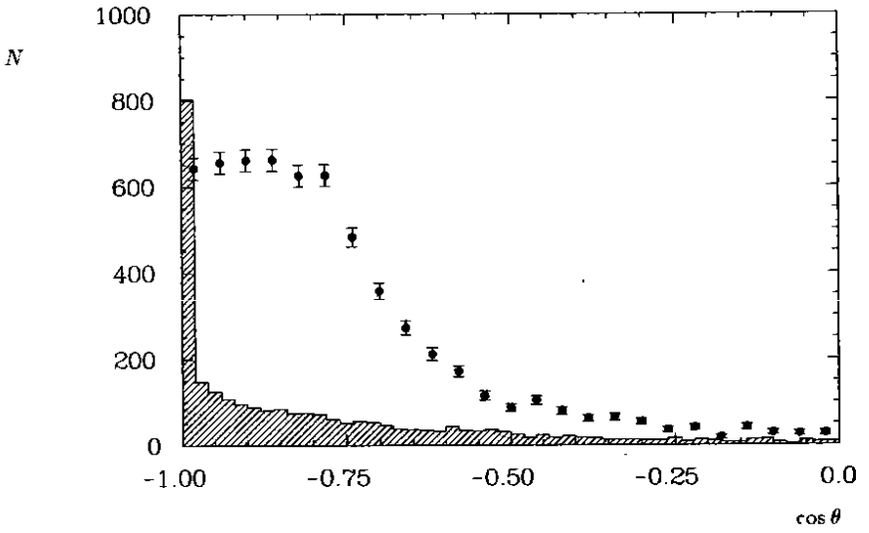

Figure 8: Distribution of the angle between $\vec{p}_{tot}$ and 1-prong direction, for data (hatched histogram) and neutrinoless τ decays (with error bars) after cuts 1 and 2

- **Cut No. 3**: A further requirement again exploits the hermeticity of the ARGUS detector. For events including a neutrinoless τ decay, the distribution of the opening angle between the charged particle on the 1-prong side and the total momentum is rather broad, while for radiative events the spectrum peaks at $\cos(\vec{p}_{1-prong}, \vec{p}_{tot}) = -1$ as shown in fig. 8. Thus, the requirement

$$\cos\,(\vec{p}_{1-prong}, \vec{p}_{tot}) > -0.95$$

reduces this background.

After these selection criteria no candidates for the decay channels $\tau^- \to \mu^-\gamma$ and $\tau^- \to \mu^-\pi^0$ survive, if the charged particle from the recoil standard τ decay is not positively identified as a muon. The latter condition specifically suppresses μ-pair events. Figure 12 shows the mass spectrum for both channels; in table 2 the efficiencies and the upper limits on the branching ratios are collected.

For the other channels of this section, four additional restrictions are imposed in order to specifically remove the background from radiative Bhabha events:

- **Cut No. 4**: For Bhabha events, the total transverse momentum of all particles with respect to the beam direction is small, while the sum of the momenta of all measured

particles is approximately equal to the center-of-mass energy. Hence, the requirement

$$\mid p_{trans} \mid > 0.5 \cdot \sum \mid \vec{p}_{measured} \mid - 0.3$$

reduces the Bhabha background (bottom right of fig. 9a) appreciably, while leaving a potential signal from neutrinoless τ decays relatively uneffected as shown in fig. 9b.

- **Cut No. 5**: The tagging 1-prong charged particle must not be identified as an electron. In addition we demand a small shower energy associated with the 1-prong, to further reduce the misidentification probability.

$$E^{shower}_{1-prong} < 0.2 \cdot E_{cm}$$

- **Cut No. 6**: Further, both charged tracks are required to be non-collinear by more than 30°:

$$\cos(1 - prong, charged\ track) > -0.86$$

- **Cut No. 7**: Analogous to cut no. 5 introduced in section 2.1, a restriction is made on the effective mass of the 1-prong side, taking into account the missing momentum four-vector. This reduces the contamination due to standard τ events and eliminates the Bhabha background in the signal region for the channels 19 – 24:

$$2\ \frac{GeV^2}{c^4} < m^2_{\tau-1-prong} < 7\ \frac{GeV^2}{c^4}$$

The resulting mass spectra for the remaining channels discussed in this section are again shown in fig. 12. By identifying the charged track as a pion, six events remain in the signal region for the channels $\tau^- \rightarrow \pi^-\gamma$ and $\tau^- \rightarrow \pi^-\pi^0$. After applying the same selection requirements to a Monte Carlo sample of τ pair events, it has been shown that these six events can be explained by the standard τ decay $\tau^- \rightarrow \rho^-\nu_\tau \rightarrow \pi^-\pi^0\nu_\tau$. Table 2 summarizes the results of the analysis.

3.3 Search for the neutrinoless decays $\tau^- \rightarrow e^-\eta$ and $\tau^- \rightarrow \mu^-\eta$

η mesons are reconstructed in the decay channel $\eta \rightarrow \gamma\gamma$ (39% branching ratio). In contrast to π^0 decays, it is almost always possible to detect the two photons separately. The contribution from η mesons forming a single cluster, accompanied by the same background as discussed in section 3.2, is small and is therefore not taken into account. After requiring a reconstructed η meson, the largest remaining background source is due to standard τ decays with two single-cluster π^0 mesons in the final state simulating an η meson. These background channels

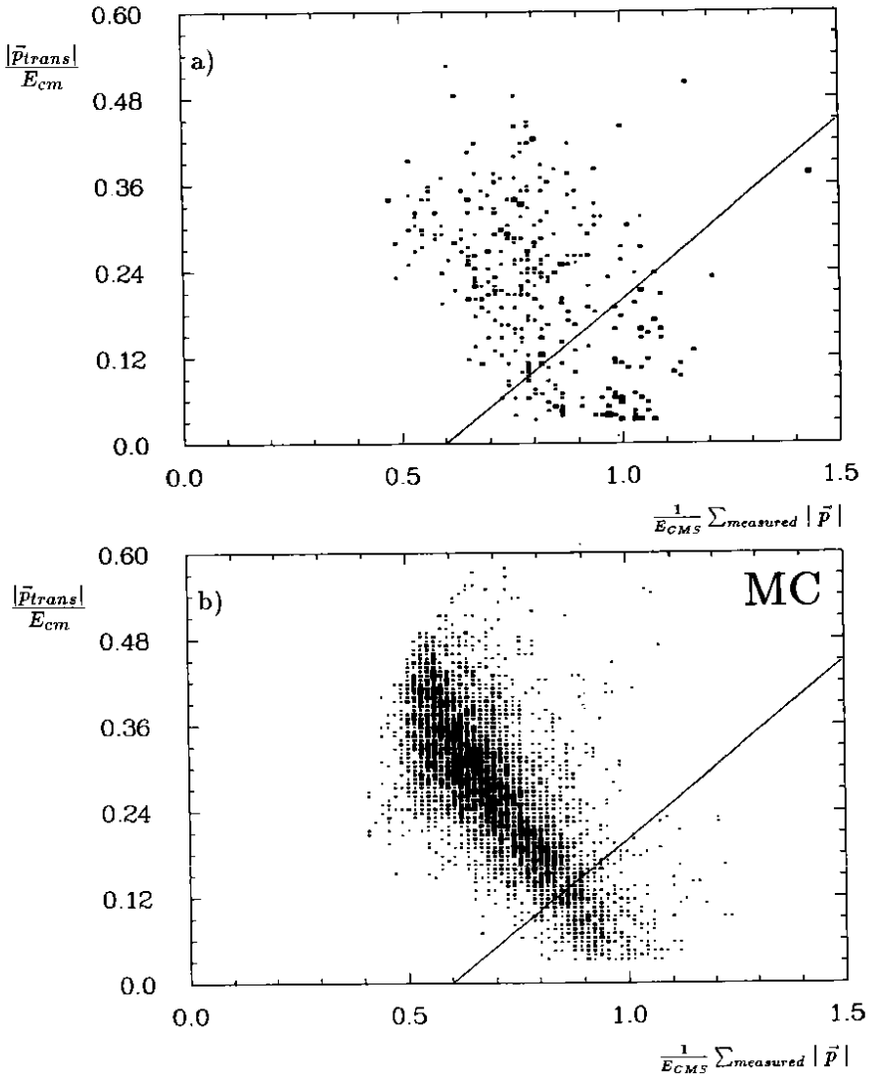

Figure 9: $\frac{1}{E_{CMS}} \mid \vec{p}_{trans} \mid$ versus $\frac{1}{E_{CMS}} \sum_{measured} \mid \vec{p} \mid$ for a) data and b) neutrinoless τ decays after cuts 1, 2 and 3. Events below the solid line are discarded.

No.	Decay channel	Cuts	ϵ_{sel}[%]	ϵ_{tot}[%]	N_{seen}	Upper limit [10^{-5}]
19.	$\tau^- \to \mu^-\gamma$	1 2 3	14.8	9.0	0	3.4
20.	$\tau^- \to \mu^-\pi^0$	1 2 3	14.8	6.9	0	4.4
21.	$\tau^- \to e^-\gamma$	1–7	4.7	2.6	0	12
22.	$\tau^- \to e^-\pi^0$	1–7	4.7	1.8	0	17
23.	$\tau^- \to \pi^-\gamma$	1–7	4.7	2.6	6	28
24.	$\tau^- \to \pi^-\pi^0$	1–7	4.7	2.0	6	37

Table 2: Summary of cuts, efficiencies and resulting upper limits (90% CL) for channels 19 – 24

are strongly reduced by identifying the charged track as an electron or a muon, which is finally combined with the reconstructed η meson and then checked for consistency with a neutrinoless decay.

The following cuts exploit the properties of the photons from an η decay, as derived by Monte Carlo studies:

- Those photons used for η reconstruction are required to have a minimum energy of

$$E_\gamma^{min} > 0.02 \cdot E_{cm}$$

to improve the η mass resolution and to suppress contributions due to bremsstrahlung.

- The opening angles between the photons from the η decay and the charged particle of the neutrinoless τ decay peak at small angles. Hence only photons within 72° of the charged track are considered for reconstructing the η:

$$\cos(\gamma, charged\ particle) > 0.3\,.$$

This cut reduces the probability of using photons from the recoiling standard τ decay.

- The invariant mass of the two photons must be compatible with the η mass:

$$\mid m(2\gamma) - m(\eta) \mid < 0.15\ GeV/c^2\,.$$

Two additional constraints are imposed on the η meson:

- From Monte Carlo studies, it has been shown that the η meson must have an opening angle with respect to the charged track which lies in the range:

$$0.5 < \cos(\eta, charged\ track) < 0.9\,.$$

No.	Decay channel	Cuts	ϵ_{sel}[%]	ϵ_{tot}[%]	N_{seen}	Upper limit [10^{-5}]
23.	$\tau^- \to e^-\eta$	s. text	8.1	4.9	0	6.3
24.	$\tau^- \to \mu^-\eta$	s. text	8.1	4.2	0	7.3

Table 3: Summary of cuts, efficiencies and resulting upper limits (90% CL)

- The mass resolution is improved, with only a marginal number of lost neutrinoless τ events, if the momentum of the η meson is restricted to the interval:

$$p(\eta) > 0.1 \cdot E_{cm}\,.$$

Events with a candidate for the decay $\tau^- \to e^-\eta$ ($\mu^-\eta$) with a well identified electron (muon) in the standard τ decay hemisphere are rejected in order to exclude background from Bhabha (μ-pair) events.

Figure 12 shows the mass spectra for these search channels. No event is observed near the τ lepton mass. The resulting upper limits on the branching fractions are given in table 3 together with the total selection efficiencies including lepton identification.

3.4 Search for the neutrinoless τ decays $\tau^- \to \bar{p}\,\gamma$ and $\tau^- \to \bar{p}\,\pi^0$

The cuts described in section 3.2 are also applied for these channels, since the Bhabha and μ-pair background is shifted into the signal region by lepton misidentification as a proton. Only those events are considered, where the charged track of the 1-prong standard τ decay is not identified as an electron.

Since the phase space for the decay $\tau^- \to \bar{p}\,\gamma$ and $\tau^- \to \bar{p}\,\pi^0$ is very small, the minimal angle between the neutral and charged particle is only 10°:

- Only photons in the angular interval of

$$0.6 < \cos(\gamma, charged\ particle) < 0.98$$

are regarded as due to a neutrinoless τ decay.

The resulting invariant mass spectrum is shown in fig. 10. For comparison the results of a Monte Carlo simulation are included for τ pair events, scaled to the known number of τ pairs in the data. The distribution is dominated by 2-prong τ events where one τ lepton decays via $\tau^- \to \rho^-\nu_\tau \to \pi^-\pi^0\nu_\tau$ and the π^- is misidentified as an anti-proton. This demonstrates that the observed mass distribution is compatible in shape and absolute rate with the expectation for this background source.

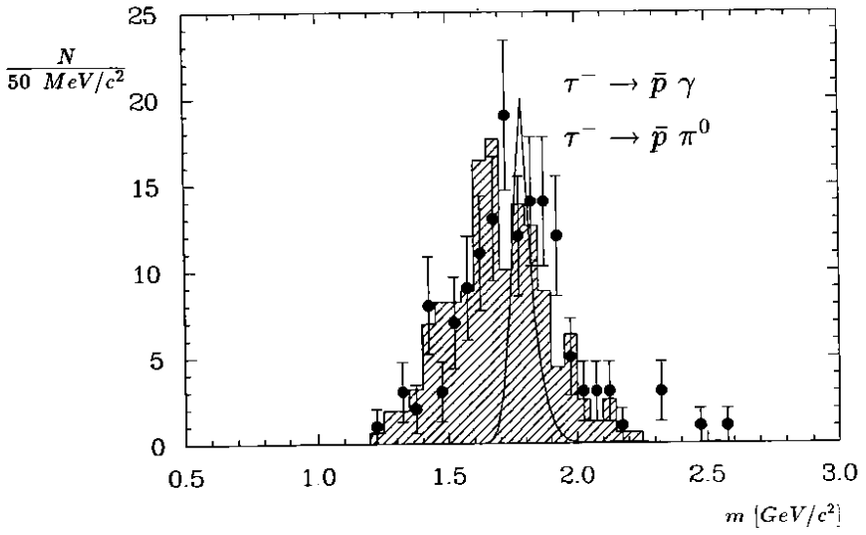

Figure 10: Invariant mass of the neutrinoless side for the decay channels $\tau^- \rightarrow \bar{p}\ \gamma$ und $\tau^- \rightarrow \bar{p}\ \pi^0$ after cuts 1 - 7 for data (with error bars), a Monte Carlo simulation of standard τ decays scaled to data (hatched histogram) and the expected resolution function for neutrinoless τ decays (solid line).

- **Cut No. 8**: This background can be reduced by a more restrictive identification of the charged track as a proton [3] and by exploiting the correlation between the proton momentum and the invariant mass of the neutrinoless side.

  As demonstrated by fig. 11a and 11b the contributions of standard τ decays are strongly suppressed by the cut

$$\frac{|\vec{p}(p)|}{E_{cm}} > -0.22 \cdot m(p\gamma) + 0.66$$

while approximately 50% of the neutrinoless τ decay channels 23 and 24 pass this condition. The final invariant mass distribution is shown in fig. 12. No event is found in the 2σ-region around the τ mass. In table 4 the efficiencies and the upper limits on the branching ratios are collected.

3.5 Search for the neutrinoless τ decay $\tau^- \rightarrow \bar{p}\ \eta$

For this channel, an identified proton and a reconstructed η meson is required, in the same way as described in section 3.3, with a slight deviation in the accepted angular range for the

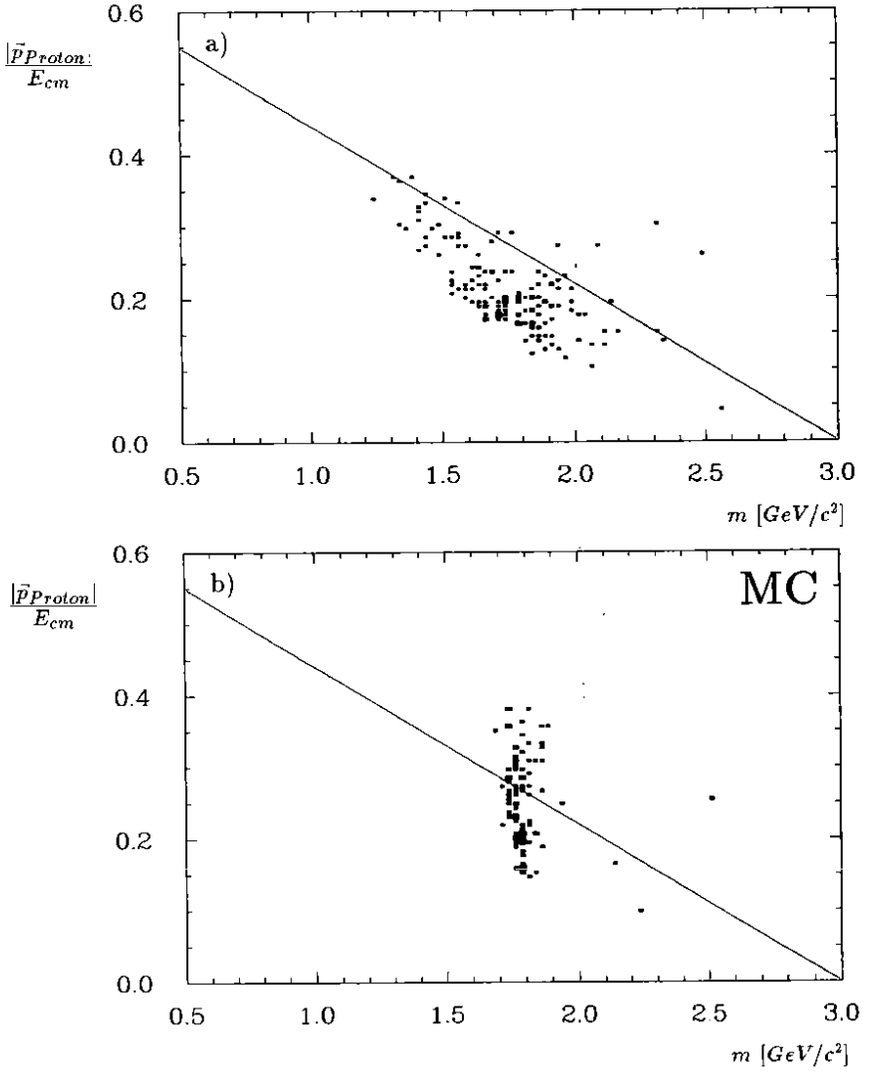

Figure 11: Proton momentum versus invariant mass of the neutral and charged particle for a) data and b) neutrinoless τ decays

No.	Decay channel	Cuts	$\epsilon_{sel}[\%]$	$\epsilon_{tot}[\%]$	N_{seen}	Upper limit $[10^{-5}]$
25.	$\tau^- \to \bar{p}\,\gamma$	1–8	6.4	1.0	0	29.0
26.	$\tau^- \to \bar{p}\,\pi^0$	1–8	6.4	0.5	0	65.5
29.	$\tau^- \to \bar{p}\,\eta$	s. text	8.1	1.7	16	129

Table 4: Summary of cuts, efficiencies and resulting upper limits (90% CL) for channels involving baryons

η meson with respect to the proton direction. Monte Carlo studies for this decay channel show that the η meson should lie within the interval:

$$0.6 < \cos(\eta, charged\ particle) < 0.98\,.$$

Being unable to apply any of the previous kinematic cuts without a large loss of efficiency, 16 events are left in the signal region between 1.7 and 1.9 GeV/c^2. Six of these are shown to be standard τ decays, where the decays $\tau^- \to a_1^-\nu_\tau \to \pi^-\pi^0\pi^0\nu_\tau$ and $\tau^- \to \rho^-\nu_\tau \to \pi^-\pi^0\nu_\tau \to \pi^-\gamma\gamma\nu_\tau$ are misidentified as the neutrinoless decay $\tau^- \to \bar{p}\,\eta$. In order to understand the nature of the remaining events, one can study the mass distribution for this channel in fig. 12. Due to the large mass of this final state, Bhabha events are shifted into the signal region where they contribute to the observed background. There is no significant enhancement close to the mass of the τ lepton. Therefore, it is concluded that there is no evidence for the decay $\tau^- \to \bar{p}\,\eta$ and that the observed events are due to background. The upper limits are obtained by subtracting the 6 known τ background events and treating the remainder as a potential signal. Table 4 contains the relevant information of the analysis.

4 Discussion and summary

The results of this analysis are compared to those of other experiments in table 5 [7,2,8,9]. The limits for the channels $\tau^- \to \mu^-\eta$, $\tau^- \to \bar{p}\,\gamma$, $\tau^- \to \bar{p}\,\pi^0$, $\tau^- \to \bar{p}\,\eta$, $\tau^- \to \pi^-\gamma$ and $\tau^- \to \pi^-\pi^0$ have been determined for the first time. Of special interest are the channels $\tau^- \to \bar{p}\,\gamma$, $\tau^- \to \bar{p}\,\pi^0$ and $\tau^- \to \bar{p}\,\eta$ where baryon and lepton number violating τ decays were investigated. No evidence for either lepton number and lepton flavour or for baryon number violation was observed. For nearly all channels the new upper limits on branching ratios represent improvements by approximately a factor of two. This was achieved by the increased size of the τ-pair sample, and through exploiting the hermeticity of the ARGUS detector. The latter allows the use of restrictions on the effective 1-prong mass for the

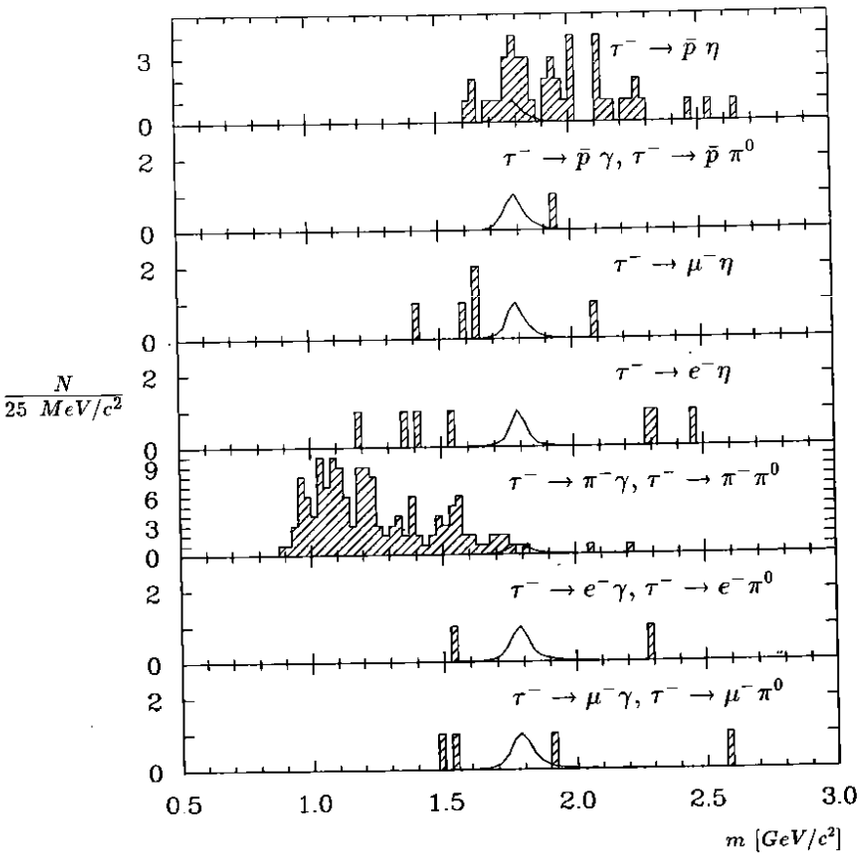

Figure 12: Invariant masses for the charged and neutral particle of the decay channels 19 – 29, with corresponding resolution function (solid line)

tagging standard τ decay as described in detail in section 2.2. Several extensions of the standard model exist which predict neutrinoless τ decays [10,11,12,13]. The new data allow to constrain the couplings and characteristic energies of these models.

Acknowledgements

It is a pleasure to thank U. Djuanda, E. Konrad, E. Michel, and W. Reinsch for their competent technical help in running the experiment and processing the data. We thank Dr. H. Nesemann, B. Sarau, and the DORIS group for excellent operation of the storage ring. The visiting groups wish to thank the DESY directorate for the support and kind hospitality extended to them.

Upper Limits $[10^{-5}]$ $(90\%CL)$						
Nr.	decay channel	MARK II	ARGUS 86	Crystal Ball	CLEO	ARGUS 91
1.	$\tau^- \to e^-e^+e^-$	40	3.8		2.7	1.3
2.	$\tau^- \to e^-\mu^+\mu^-$	33	3.3		2.7	1.9
3.	$\tau^- \to e^+\mu^-\mu^-$				1.6	1.8
4.	$\tau^- \to \mu^-e^+e^-$	44	3.3		2.7	1.4
5.	$\tau^- \to \mu^+e^-e^-$				1.6	1.4
6.	$\tau^- \to \mu^-\mu^+\mu^-$	49	2.9		1.7	1.9
7.	$\tau^- \to e^-\pi^+\pi^-$		4.2		6.0	2.7
8.	$\tau^- \to e^+\pi^-\pi^-$				1.7	1.8
9.	$\tau^- \to \mu^-\pi^+\pi^-$		4.0		3.9	3.6
10.	$\tau^- \to \mu^+\pi^-\pi^-$				3.9	6.3
11.	$\tau^- \to e^-\rho^0$	37	3.9			1.9
12.	$\tau^- \to \mu^-\rho^0$	44	3.8			2.9
13.	$\tau^- \to e^-\pi^+K^-$		4.2		5.8	2.9
14.	$\tau^- \to e^+\pi^-K^-$				4.9	2.0
15.	$\tau^- \to \mu^-\pi^+K^-$		12		7.7	11
16.	$\tau^- \to \mu^+\pi^-K^-$				4.0	5.8
17.	$\tau^- \to e^-K^{*0}$	130	5.4			3.8
18.	$\tau^- \to \mu^-K^{*0}$	100	5.9			4.5
19.	$\tau^- \to e^-\gamma$	64		20		12
20.	$\tau^- \to e^-\pi^0$	210		14		17
21.	$\tau^- \to \mu^-\gamma$	55				3.4
22.	$\tau^- \to \mu^-\pi^0$	82				4.4
23.	$\tau^- \to e^-\eta$			24		6.3
24.	$\tau^- \to \mu^-\eta$					7.3
25.	$\tau^- \to \bar{p}\,\gamma$					29.0
26.	$\tau^- \to \bar{p}\,\pi^0$					65.5
27.	$\tau^- \to \pi^-\gamma$					28
28.	$\tau^- \to \pi^-\pi^0$					37
29.	$\tau^- \to \bar{p}\,\eta$					129

Table 5: Comparison of extracted limits with results from previous experiments

References

[1] J.J. Simpson, Phys. Rev. Lett **54** (1985) 1891
A. Hime und N. A. Jelley, Phys. Lett. **B257** (1991) 441

[2] H. Albrecht et al. (ARGUS) Phys. Lett. **185B** (1987) 228

[3] D. Töpfer, Diploma thesis, Universität Dortmund (1991),
Internal Report, DESY F15-92-01 (1992)

[4] H. Albrecht et al. (ARGUS), Nucl. Instr. Meth. **A275** (1989) 1

[5] S. Weseler, Doctor thesis, Universität Heidelberg (1986)

[6] B. Spaan, Doctor thesis, Universität Dortmund (1988)

[7] K. G. Hayes et al. (MARK II), Phys. Rev. **D25** (1982) 2869

[8] S. Keh et al. (Crystal Ball), Phys. Lett. **212B** (1988) 123

[9] T. Bowcock et al. (CLEO), Phys. Rev. **D41** (1990) 805

[10] A. Masiero, Preprint DFPD/90/TH732 (1990)

[11] R. Arnowitt, P. Nath, Phys. Rev. Lett. **66** (1991) 2708

[12] S. Kelley, J. L. Lopez, D. V. Nanopolous and H. Pois, Nucl. Phys. **B358** (1991) 27

[13] M.C. Gonzalez-Garcia, J.W.F. Valle, Preprint FTUV/91-12 (1991)